NeuroImage: Clinical 24 (2019) 102083

Contents lists available at ScienceDirect

NeuroImage: Clinical

journal homepage: www.elsevier.com/locate/ynicl

Psychopathy is associated with shifts in the organization of neural networks in a large incarcerated male sample

Scott Tillem[a,*], Keith Harenski[b], Carla Harenski[b], Jean Decety[c], David Kosson[d], Kent A. Kiehl[b,e], Arielle Baskin-Sommers[a]

[a] Yale University, Department of Psychology, 2 Hillhouse Ave. New Haven, CT 06511, USA
[b] Mind Research Network, Albuquerque, NM USA
[c] University of Chicago, Department of Psychology and Department of Psychiatry and Behavioral Neuroscience, Chicago, IL USA
[d] Rosalind Franklin University of Medicine and Science, Department of Psychology, Chicago, IL USA
[e] University of New Mexico, Department of Psychology, Albuquerque, NM USA

ARTICLE INFO

Keywords:
Psychopathy
Resting state
Graph analysis
Minimum spanning tree
Dorsal attention network
Subcortical structures

ABSTRACT

Psychopathy is a personality disorder defined by antisocial behavior paired with callousness, low empathy, and low interpersonal emotions. Psychopathic individuals reliably display complex atypicalities in emotion and attention processing that are evident when examining task performance, activation within specific neural regions, and connections between regions. Recent advances in neuroimaging methods, namely graph analysis, attempt to unpack this type of processing complexity by evaluating the overall organization of neural networks. Graph analysis has been used to better understand neural functioning in several clinical disorders but has not yet been used in the study of psychopathy. The present study applies a minimum spanning tree graph analysis to resting-state fMRI data collected from male inmates assessed for psychopathy with the Hare Psychopathy Checklist-Revised (n = 847). Minimum spanning tree analysis provides several metrics of neural organization optimality (i.e., the effectiveness, efficiency, and robustness of neural network organization). Results show that inmates higher in psychopathy exhibit a more efficiently organized dorsal attention network (β = =0.101, $p_{corrected}$ = =0.018). Additionally, subcortical structures (e.g., amygdala, caudate, and hippocampus) act as less of a central hub in the global flow of information in inmates higher in psychopathy (β = =−0.104, $p_{corrected}$ = =0.048). There were no significant effects of psychopathy on neural network organization in the default or salience networks. Together, these shifts in neural organization suggest that the brains of inmates higher in psychopathy are organized in a fundamentally different way than other individuals.

1. Introduction

Psychopathic individuals display a chronic and flagrant disregard for the welfare and rights of others through their callous, manipulative, and amoral behavior. Psychopathic individuals commit two to three times more crimes than non-psychopathic individuals, recidivate at a much higher rate, and are responsible for a disproportionate share of the annual costs associated with crime in the United States (Kiehl and Hoffman, 2011). Across different theoretical models of psychopathy, including the low-fear model (Lykken, 1957), the integrated emotion systems model (Blair, 2006), the response modulation model (Gorenstein and Newman, 1980), the attention bottleneck model (Baskin-Sommers et al., 2011a), and the paralimbic dysfunction model (Kiehl, 2006), the chronic and costly behaviors of these individuals is attributed to disruptions in information processing. Stemming from these models, decades of programmatic research highlight that psychopathic individuals display aberrancies in two general domains of information processing: emotion and attention.

One of the most studied domains of information processing in psychopathy is that of emotion processing. Psychopathic individuals show deficits in fear conditioning (see Hoppenbrouwers et al., 2016 for a meta-analytic review), emotion recognition (see Dawel et al., 2012 and Wilson et al., 2011 for meta-analytic reviews), and emotion-modulated startle to unpleasant pictures (Baskin-Sommers et al., 2013b; Patrick et al., 1993; Sadeh and Verona, 2012; Vaidyanathan et al., 2011). Additionally, psychopathic individuals show blunted cortico-limbic engagement during moral decision-making (Decety et al., 2015; Glenn et al., 2009; Harenski et al., 2014), aversive conditioning

* Corresponding author.
E-mail address: scott.tillem@yale.edu (S. Tillem).

https://doi.org/10.1016/j.nicl.2019.102083
Received 21 August 2019; Received in revised form 1 November 2019; Accepted 6 November 2019
Available online 09 November 2019

(Birbaumer et al., 2005), affective perspective taking (Sommer et al., 2010), and in response to empathogenic and facial emotion stimuli (Decety et al., 2013a, 2014, 2013b; Deeley et al., 2006; Hyde et al., 2014; Meffert et al., 2013). Overall, there is substantial evidence that psychopathic individuals display dysfunction in emotion processing that impairs their ability to orient to and process salient affective content.

Moreover, examinations of neural communication in psychopathy find that psychopathic individuals show reduced connectivity, at rest and during tasks, between structures within the default (Pujol et al., 2011; Sethi et al., 2015; Yoder et al., 2015) and salience (i.e., salience/ventral attention) networks (Espinoza et al., 2018; Yoder et al., 2015). The default network is important for socio-emotional processing (Jack et al., 2013; Spreng and Grady, 2010; Spreng et al., 2009), whereas the salience network is important for automatic orienting to salient (e.g., affective) stimuli (Corbetta and Shulman, 2002; Vossel et al., 2014). For example, Pujol et al. (2011) found that, at rest, psychopathy was associated with reduced functional connectivity between the medial prefrontal cortex and the precuneus, two major nodes of the default network. Similarly, Yoder et al. (2015) found that, during a moral reasoning task, psychopathy was associated with reduced functional connectivity between the right temporoparietal junction, a structure associated with the default network, and bilateral inferior parietal lobules, structures associated with the salience network. Collectively, these findings suggest that neural communication within and between networks critical to automatically orienting to and processing socio-emotional information may be disrupted in psychopathy.

Another domain of information processing studied in psychopathy is that of attention. There is evidence that psychopathic individuals show abnormalities in the appropriate deployment of attentional resources to notice and integrate contextual information. For example, during attention tasks (e.g., Flanker, attention blink) individuals higher in psychopathy reliably exhibit superior performance when asked to attend to goal-relevant information while ignoring goal-irrelevant distractors (Hiatt et al., 2004; Hoppenbrouwers et al., 2015; Wolf et al., 2012; Zeier et al., 2009). As another example, during affective processing tasks in which affective information is goal-relevant, individuals higher in psychopathy show intact, or even enhanced, affective responses (Baskin-Sommers et al., 2011a, 2013b; Decety et al., 2013a; Larson et al., 2013; Newman et al., 2010; Schultz et al., 2016; Tillem and Baskin-Sommers, 2018; Tillem et al., 2016), but, when affective information is goal-irrelevant, they exhibit blunted affective responses (Baskin-Sommers et al., 2011a, 2013b; Larson et al., 2013; Newman et al., 2010). Across all of these experimental paradigms, psychopathic individuals show an enhanced ability to respond to goal-relevant information while ignoring distracting, goal-irrelevant stimuli (e.g., quickly and accurately responding to targets during a flanker-type task, while effectively ignoring goal-irrelevant distractors; Zeier et al., 2009). However, sometimes screening out information beyond the immediate goal appears to come at a cost (e.g., failing to process threat-predicting cues when those cues are not directly relevant to their current goal; Baskin-Sommers et al., 2011a).

Prior research on the impact of psychopathy on cortical networks related to top-down allocation of attention, such as the dorsal attention network (Corbetta and Shulman, 2002; Vossel et al., 2014), has been limited. Whole-brain analyses show that psychopathy is associated with aberrant connectivity between dorsal attention network structures and structures outside this network at-rest (Espinoza et al., 2018) and during tasks (Yoder et al., 2015). For example, Yoder et al. (2015) found that, during a moral reasoning task, psychopathy was associated with reduced connectivity between the superior parietal sulcus (a structure associated with the dorsal attention network) and the right temporoparietal junction. However, there has not been research looking at the impact of psychopathy on neural communication within the dorsal attention network, specifically. Overall, there is clear evidence of attention abnormalities in psychopathy using behavioral and some psychophysiological (e.g., startle, EEG, and fMRI; Baskin-Sommers et al., 2013b; Larson et al., 2013; Tillem et al., 2019) measures, but neuroimaging data specifying the nature of attention-related network abnormalities is limited.

Information processing abnormalities in psychopathy are clearly complex, spanning multiple processing domains and reflected in various neural structures. Recent advances in neuroimaging methods attempt to unpack complex information processing abnormalities. Specifically, graph analysis uniquely allows researchers to examine the overall organization of information flow within entire networks and provide metrics that directly quantify how that network organization may impact the completeness, efficiency, and robustness (i.e., the optimality) of information processing (Bullmore and Sporns, 2009; Reijneveld et al., 2007; Smit et al., 2016; Stam and Reijneveld, 2007; Stam et al., 2014; Tewarie et al., 2015). Graph analytic approaches have been used to examine neural information processing disruptions in a variety of different clinical populations (e.g., schizophrenia, alcohol use disorder, autism spectrum disorder; Itahashi et al., 2014; Liu et al., 2008; Sjoerds et al., 2017). However, these methods have not been applied to understanding the complex information processing atypicalities present in psychopathy.

To test whether psychopathy quantifiably impacts neural network organization and, therefore, alters the optimality of neural information processing, we completed a minimum spanning tree (MST) graph analysis of resting-state fMRI (rs-fMRI) data collected from a large sample of male inmates. We used an incarcerated sample because individuals higher in psychopathy account for approximately 25% of incarcerated individuals (vs. 1% of the general population; Neumann and Hare, 2008); and the range of psychopathy scores represented in incarcerated samples provides appropriate controls for commonalities in experiences ranging from engagement in criminal behavior to exposure to the corrections environment that may impact neural measures. We implemented MST analysis because it provides several metrics of neural network organization that may inform our understanding of the optimality of neural information processing in psychopathy. Additionally, MST analysis has two key advantages over alternative graph analysis methods. First, other graph analysis methods require the use of an arbitrary strength threshold (or set of thresholds) during graph construction, which can alter the findings of the analysis depending on the arbitrary threshold(s) selected. In contrast, MST analyses have a fixed number of edges (i.e., connections) included during graph construction allowing for more reliable and valid evaluations of network optimality (Reijneveld et al., 2007; Smit et al., 2016; Stam and Reijneveld, 2007; Stam et al., 2014; Tewarie et al., 2015). Second, other graph analysis methods produce graphs containing a variable number of edges across individuals, biasing between-graph comparisons by artificially inflating the likelihood of finding between-graph differences. MST analyses, however, produce graphs with a fixed number of edges across individuals, allowing for unbiased comparisons of neural organization between individuals (e.g., individuals at differing levels of psychopathy; Gonzalez et al., 2016; Reijneveld et al., 2007; Smit et al., 2016; Stam and Reijneveld, 2007; Stam et al., 2014; Tewarie et al., 2015; Tillem et al., 2018). Given these advantages, MST analysis provided a robust means to evaluate the relationship between psychopathy and the optimality of neural network organization.

Based on previous research linking psychopathy with disruptions in information processing impacting socio-emotional processes and allocation of attention, we focused our initial analyses on the default, salience, and dorsal attention networks. Given prior research on emotion processing dysfunctions in psychopathy, we hypothesized that inmates higher in psychopathy would be characterized by less optimal default and salience network organization. By contrast, given existing evidence indicating enhanced attention to goal-relevant information among individuals higher on psychopathy, we hypothesized that inmates higher in psychopathy would exhibit a more optimally organized dorsal

Table 1
Full Sample Characteristics and Zero-Order Correlations (N = 945).

Variable	n	Mean	Std. Dev.	Min	Max	Correlations					
						1	2	3[†]	4	5	6
1. Age	945	33.22	8.80	18.00	62.00	—	0.05	−0.04	−0.06	−0.02	0.04
2. IQ	911	97.18	13.46	66.00	137.00		—	−0.33**	0.04	0.02	0.04
3. Race[†]	939							—	0.02	0.01	0.01
White	387										
Black	197										
Hispanic	307										
Other	48										
4. PCL-R	893	22.39	7.22	3.20	40.00				—	0.15**	0.10*
5. SUD	903	1.66	1.49	0.00	8.00					—	0.21**
6. TBI	903	0.67	1.12	0.00	15.00						—

PCL-R = Psychopathy Checklist Revised Total Score; IQ = Total IQ score on the Wechsler Adult Intelligence Scale III; SUD = Number of different substance use disorder diagnoses an inmate has met diagnostic criteria for as assessed by the Structured Clinical Interview for DSM-IV; TBI: Total number of head injuries an inmate reported in their lifetime.

* $p < 0.01$.

** $p < 0.001$.

† Spearman correlations were used to examine the effect of Race (contrast-coded, white vs. non-white).

attention network. Finally, there is recent work linking aspects of psychopathy to shifts in the structural organization of the brain (particularly within the frontal lobe; Yang et al., 2012) that may impact global (i.e., whole-brain) neural communication (Tillem et al., 2018). Therefore, we conducted an exploratory whole-brain MST analysis to evaluate the impact of psychopathy on both whole-brain neural optimality and the organizational centrality of various neural networks to global information flow.

2. Methods and materials

2.1. Participants

Participants were 945 male inmates, between the ages of 18 and 62 (M = 33.2 years old; SD = =8.8 years), incarcerated in one of eight prisons in the states of New Mexico and Wisconsin (see Table 1 for full sample characteristics). Inmates who performed below the fourth-grade level on a standardized measure of reading (Wide Range Achievement Test-III; Wilkinson, 1993), had a history of medical problems that could have either precluded clear data acquisition using fMRI (e.g., pacemaker, head injury with loss of consciousness over 30 min) or impacted their comprehension of the study materials (e.g., uncorrectable auditory or visual deficits), or were currently taking antipsychotic medications or were diagnosed with a psychotic disorder were excluded. This study was approved by the Institutional Review Board (IRB) at the University of Wisconsin-Madison and by Ethical and Independent Review (E&I) for the Mind Research Network. All participants provided informed consent and were paid at a rate commensurate with the institutions compensation for work assignments at their facility.

The Mind Research Network aims to establish a large database of neurobiological data collected in incarcerated samples. The data from the current sample were from this database and overlap with samples used in previous studies (e.g., all participants in the current study were also used by Espinoza et al., 2018). However, while prior studies with this data have examined the impact of psychopathy on specific neural connections, the current analysis is unique and optimized for a novel investigation into the impact of psychopathy on neural network organization. No other research has addressed the questions or implemented the methods used in the present study.

2.2. Measures

2.2.1. Psychopathy checklist-revised (PCL-R; Hare, 2003)

All participants were evaluated for psychopathy using the PCL-R, which utilizes information gathered from institutional records and an interview to rate inmates on the presence of 20 different psychopathic traits. Each trait was scored on a scale ranging from 0 to 2 depending upon the degree to which that trait was present in the individual. Total scores range from 0 to 40. Inter-rater reliability was available for 9% of the current sample. The interclass correlation for these double ratings was 0.917.

2.2.2. Covariates

All participants were assessed on a brief measure of IQ (Wechsler Adult Intelligence Scale III; Wechsler, 1997). All participants also were assessed for substance use disorders using the Structured Clinical Interview for DSM-IV (First et al., 2002), and a history of head injuries using a modified version of the Rivermead Post-Concussion Symptoms Questionnaire (King et al., 1995) or a head injury/loss of consciousness questionnaire (*Note*: different protocols were used to assess TBI at different data collection sites, with n = 701 being assessed using the Rivermead Post-Concussion Symptoms Questionnaire and n = 202 being assessed with an in-house head injury/loss of consciousness questionnaire). Participants who had missing data for any of these measures were excluded from data analysis, leaving a sample of n = 849.

2.3. Imaging procedures and processing

All participants completed an rs-fMRI session that was at least 5-minutes long. A subset of the sample (n = 142) completed 10-minute (n = 84) or 15-minute (n = 58) resting-state sessions (instead of the standard 5-minute resting-state session). The data for those participants were truncated so that only the first 5-minutes of their fMRI scan was used in the current analysis; this was done to ensure that all participants had the same amount of data examined.

During the rs-fMRI session, participants were asked to lay still, look at a fixation cross, and keep their eyes open. Compliance with instructions was monitored by eye tracking.

2.3.1. Imaging parameters

Resting-state fMRI data were collected on site at the prisons using a mobile Siemens 1.5T Avanto scanner with advanced SQ gradients (max slew rate 200T/m/s, 346T/m/s vector summation, rise time 200μs) equipped with a 12-element head coil. The EPI gradient-echo pulse sequence (TR = =2000 ms; TE = =39 ms; flip angle 75°; FOV 24 × 24 cm; 64 × 64 matrix; 3.4 × 3.4 mm-inplane resolution; 4 mm slice thickness; 1 mm gap; 27 slices) effectively covered the entire brain

(150 mm) in 2.0 s. Padding and head restraints were used to minimize head motion.

2.3.2. Node identification

Cortical nodes in our analysis were defined by the Schaefer 300 parcel atlas (Schaefer et al., 2018), and were organized into seven different cortical networks (Yeo et al., 2011). The Schaefer et al. (2018) atlas was developed to apply aspects of both local gradient and global similarity parcellation approaches; this integrative approach produced more homogeneous parcels than other parcellation methods, and allowed for optimal identification of distinct, neurobiologically meaningful parcels.

Since the Schaefer et al. (2018) atlas is limited to the cortical surface, subcortical nodes from another atlas were needed to supplement it. Moreover given the difficulties involved in functionally parcellating subcortical structures (Gordon et al., 2016; Kong et al., 2018; Pauli et al., 2018; Schaefer et al., 2018; Yeo et al., 2011), an anatomical atlas was used to supplement the Schaefer et al. (2018) atlas with subcortical nodes. Following prior research examining neural connectivity in antisocial samples (Lindner et al., 2018), we used the AAL atlas to identify 14 anatomically defined subcortical nodes, including the right and left amygdala, hippocampus, parahippocampus, caudate, putamen, pallidum, and thalamus (Tzourio-Mazoyer et al., 2002).

2.3.3. Preprocessing

Functional data were processed using the Statistical Parametric Mapping software (SPM12, http://www.fil.ion.ucl.ac.uk/spm/). Despiking was performed using the ArtRepair toolbox to remove images with severe artifacts (Mazaika et al., 2009). Additionally, the time point of each spike was extracted for use as an independent regressor during the subsequent denoising procedures. Functional images were then realigned using INRIAlign an algorithm that is unbiased by local signal changes (Freire and Mangin, 2001; Freire et al., 2002). The images were then spatially normalized to MNI space (Calhoun et al., 2017) and smoothed using a 6 mm FWHM Gaussian kernel. Following preprocessing, two participants were excluded from subsequent analyses because more than 20% of their time course was identified as artifact during despiking, leaving a final sample of $n = 847$.

2.3.4. Connectivity analysis

A region of interest (ROI) to ROI connectivity analysis was conducted on the preprocessed data using the Conn toolbox (Whitfield-Gabrieli and Nieto-Castanon, 2012). More specifically, preprocessed rs-fMRI data were extracted from the ROIs (i.e., nodes) for this analysis. Denoising procedures were then applied to the data including: 1) orthogonalizing the time courses with respect to signal in the white matter and CSF, the six-realignment parameters, the 1st- and 2nd-order derivatives of each realignment parameter, and the despiking regressors (for each spike identified during despiking, an independent regressor was used where the time point of the spike was coded as 1 and all other time points were coded a 0); 2) band-pass filtering (.008Hz-0.09 Hz); and, 3) cubic detrending. This multi-step denoising procedure reduced signal artifact originating from CSF and white matter, censored signal produced by excessive motion, thereby greatly reducing the impact of motion artifact on the data, and mitigated signal artifact due to biological noise (e.g., breathing, heart rate, etc., Power et al., 2014; Siegel et al., 2016; Whitfield-Gabrieli and Nieto-Castanon, 2012). Following denoising, the connectivity analysis was performed using the Conn toolbox ROI to ROI first-level static connectivity analysis procedure (Whitfield-Gabrieli and Nieto-Castanon, 2012). This procedure generated pairwise correlations between each individual's time course for each pair of ROIs, ultimately producing a whole-brain connectivity matrix for each participant. Following the connectivity analysis, connectivity matrices for each network of interest for the within-network analyses (i.e., default, salience, and dorsal attention networks) were extracted from the whole-brain connectivity matrix. All matrices were then inversed (i.e., inversed matrix = 1-matrix), assigning the smallest values to the shortest distances (i.e., the strongest connections) between nodes in the network. This procedure was necessary for a robust estimation of a highly connected and efficient subnetwork in the subsequent MST analysis.

2.3.5. MST analysis

Following the connectivity analysis, MSTs were generated in MATLAB ("graphminspantree" function; https://www.mathworks.com/help/releases/R2016a/bioinfo/ref/graphminspantree.html) for each participant's four connectivity matrices (i.e., default matrix, salience matrix, dorsal attention matrix, and whole-brain matrix) using the Kruskal algorithm (Kruskal, 1956). An MST is a sub-graph where all nodes are connected (either directly or indirectly) to all other nodes in the network, but which contains no loops. All MST graphs with a specific number of nodes (N) have the same number of edges (E; $E = N$-1), allowing for unbiased between graph comparisons without the need to set arbitrary strength thresholds (Reijneveld et al., 2007; Smit et al., 2016; Stam and Reijneveld, 2007; Stam et al., 2014; Tewarie et al., 2015). The Kruskal algorithm constructs these MSTs by ordering all the possible edges in sequence from least costly (i.e., the strongest connection) to most costly (i.e., the weakest connection). Then the algorithm goes down that list of possible edges adding each edge to the graph until the MST graph is complete (i.e., until $E = N$-1). During this process, if the algorithm comes across an edge that would create a loop, it skips that edge and continues to the next edge on the list.

Following MST construction, metrics of network optimality and organization were extracted from each MST for each participant in MATLAB utilizing a combination of native MATLAB functions, the MIT graph toolbox (http://strategic.mit.edu/downloads.php?page=matlab_networks), and custom MATLAB scripts. MST metrics were then natural log transformed prior to data analysis (Gonzalez et al., 2016; Smit et al., 2016).

2.3.6. MST metrics

2.3.6.1. Within-network analyses. For each of the within-network analyses, eight metrics of network organization were extracted. Each of these eight metrics reflect different aspects of network optimality (see Table 2 for descriptions).

2.3.6.2. Whole-brain analyses. For the whole-brain analysis, in addition to the eight metrics of network optimality used in the within-network analyses, two metrics of global organization were extracted from the whole-brain MSTs for each network in the whole-brain organization analysis (i.e., the default network, salience network, dorsal attention network, cognitive control network, somatosensory/motor network, limbic network, visual network, and subcortical structures; see Table 2 for descriptions of the organizational metrics).

2.4. Data reduction and analysis

2.4.1. Factor analysis

Given the large number of metrics of interest in the network optimality analyses, a whole-brain exploratory factor analysis (EFA) with oblimen rotation was conducted to explore the common associations between the eight MST metrics of network optimality. This analysis was conducted to minimize the number of comparisons and, thereby, reduce the risk for Type I error. Factors were extracted using a principle component analysis, which yielded three factors with eigenvalues greater than one, accounting for 88.00% of the total variance of the MST network optimality metrics (see Table 3).

Factor 1 (eigenvalue = 3.50) was primarily driven by metrics related to the number of edges information may need to travel through during neural communication (i.e., efficiency; ECC_{mean}, Diameter, and ASP). Factor 2 (eigenvalue = 2.42) was primarily driven by metrics related to how much information is traveling through a single,

Table 2
Descriptions of MST Metrics.

Metric	Definition	Description: Optimality Analyses	Description: Global Organization Analysis
Degree	Ratio of the number of edges connected to a specific node (*e*) to the total number of possible edges connected to a single node (Degree = *e/E*).	MSTs with higher $Degree_{max\_global}$ have larger largest "hubs" (i.e., largest hubs with a greater number of connections), and thus can more effectively integrate information between network structures.	Networks or sets of structures with higher $Degree_{mean\_local}$ act as more of a hub in the global flow of information, and thus are more important for global information integration.
Eccentricity (*ECC*)	Ratio of the longest distance between a specific node and any other node in the MST (*ecc*) to the longest possible distance between any two nodes in the MST (*ECC = ecc/E*).	MSTs with lower ECC_{mean} have shorter longest paths, on average, allowing information to be more efficiently communicated throughout the network, even between distally connected nodes.	—
Betweenness centrality (*BC*)	Ratio of the number of shortest paths passing through a specific node (*C*) to the total number of possible shortest paths passing through a specific node in the MST (*BC = C/E*[E-1]*).	MSTs with higher BC_{max_global} have more information traveling through a single, centrally located hub, allowing for both efficient communication and effective information integration, but also leaving the MST vulnerable if this central hub were damaged or overloaded.	Networks or sets of structures with higher BC_{mean_local} have more information passing through them (i.e., are more central) in the global flow of information, and thus have more influence on global neural communication and information processing.
Kappa	A measure of the variance in the degree of nodes (*e*) throughout the MST.	MSTs with higher Kappa have greater variability in the number of connections across nodes, allowing for greater information integration within the network.	—
Diameter	Ratio of the longest shortest path in the MST (*D*) to the longest possible distance between any two nodes in the MST (Diameter = *D/E*).	MSTs with smaller diameters are more tightly organized, allowing information to be transferred between the two most distal nodes of the network more efficiently.	—
Leaf Fraction	The ratio of the number of leafs in the MST (*L*) to the maximum possible number of leafs in the MST (Leaf Fraction = *L/[N-1]*).	MSTs with higher leaf fractions have fewer hubs, but those hubs are, on average, proportionally larger (in terms of their raw number of connections), allowing for greater information integration within the network.	—
Average Shortest Path (*ASP*)	Average shortest path length between all possible combinations of nodes within a network.	MSTs with smaller ASP require information to, on average, travel through fewer connections to get from any node to any other node in the network, allowing for more efficient neural communication.	—
Tree Hierarchy (*Th*)	A metric examining the balance of efficiency, hubness, and vulnerability within a network (Th = $L/[2E^{*}BC_{max\_global}]$).	MSTs with larger Th exhibit a more optimal balance of efficient neural communication, centralized information integration, and vulnerability, allowing for robust network functioning across a variety of situations (e.g., high processing demand, stroke, etc.).	—

N = Total number of nodes in an MST; *E* = Total number of edges in an MST (*E* = *N* – 1).

Table 3
Pattern Matrix for the Principle Component Analysis after Oblimen Rotation.

Variable	Factor 1 (Efficiency)	Factor 2 (Vulnerability)	Factor 3 (Hubness)
ASP†	0.928	−0.056	0.052
ECC_{mean}†	0.992	−0.054	−0.034
Diameter†	0.984	−0.020	−0.044
BC_{max_global}	0.166	−0.897	0.197
Th	−0.026	0.950	0.197
$Degree_{max\_global}$	−0.120	−0.202	0.847
Leaf Fraction	0.206	0.359	0.666
Kappa	0.124	0.156	0.883

† Reversed Coded.

centralized node, and the vulnerability of the network should that node be knocked out (i.e., vulnerability; *Th* and BC_{max_global}). Factor 3 (eigenvalue = 1.12) was primarily driven by metrics related to the size and number of hubs throughout the network (i.e., hubness; $Degree_{max\_global}$, Leaf Fraction, and Kappa). Of note, these three factors map onto higher-order network properties well established in the prior literature (Reijneveld et al., 2007; Smit et al., 2016; Stam and Reijneveld, 2007; Stam et al., 2014; Tewarie et al., 2015). These three factors were extracted and used for all within-network and whole-brain network optimality analyses. Moreover, to ensure that these factors were comparable across analyses, the whole-brain factor loadings were used to extract these three factors for each of the within-network analyses.

2.4.2. Data analysis

Separate linear regression models were run using a robust regression procedure for each of the dependent variables of interest (i.e., the three factor scores for each of the within-network analyses and the whole-brain optimality analysis, as well as, the local metrics for the whole-brain organization analysis). In each of these models, PCL-R total score (z-scored) was the primary predictor of interest. Additionally, race (contrast-coded, white vs. non-white), number of substance use disorder diagnoses (SUD; z-scored), age (z-scored), IQ (z-scored), and number of previous head injuries (TBI; z-scored) were included as simultaneous covariates in the models. Race was included since previous research studies on psychopathy show different neurocognitive profiles across races (Baskin-Sommers et al., 2013a, 2011b). SUD and TBI were included because both were correlated with PCL-R scores in the current sample (see Table 1) and have been linked with abnormalities in neural network organization and functioning (Caeyenberghs et al., 2012; Liu et al., 2009; Pandit et al., 2013). Age and IQ were included in the models because both have been associated with differences in several of

the network metrics of interest for these analyses (Langer et al., 2012; Neubauer and Fink, 2009; Smit et al., 2016; see Supplementary Table 1 for zero-order correlations between all covariates and dependent variables of interest in the final sample, $n = 847$).

All β-values were Bonferroni corrected within each analysis (e.g., β-values were corrected within the default network analysis, salience network analysis, dorsal attention network analysis, whole-brain optimality analysis, and the whole-brain organization analysis). *P*-values within the Results section are corrected *p*-values; Tables 4–9 show both the uncorrected and corrected *p*-values.

Table 4
Within-Network Optimality Regression Analyses: Default Network.

	β	Std. Err.	*t*	*p*	$p_{corrected}$ †
Efficiency Factor					
Overall model: $F(6,840) = 1.31$, $p = 0.250$					
PCL-R	0.062	0.037	1.69	0.092	0.276
SUD	−0.028	0.037	−0.75	0.455	1.000
Age	0.054	0.036	1.50	0.133	0.399
Race	−0.034	0.038	−0.89	0.376	1.000
IQ	0.011	0.038	0.30	0.767	1.000
TBIs	−0.046	0.037	−1.23	0.219	0.657
Constant	0.016	0.036	0.45	0.653	1.000
Vulnerability Factor					
Overall model: $F(6,840) = 2.37$, $p = 0.028$					
PCL-R	−0.076	0.036	−2.13	0.033	0.099
SUD	−0.028	0.036	−0.77	0.444	1.000
Age	−0.072	0.035	−2.02	0.043	0.129
Race	−0.058	0.037	−1.55	0.121	0.363
IQ	−0.021	0.037	−0.56	0.576	1.000
TBIs	0.074	0.036	2.05	0.041	0.123
Constant	0.011	0.035	0.31	0.758	1.000
Hubness Factor					
Overall model: $F(6,840) = 1.83$, $p = 0.090$					
PCL-R	0.064	0.036	1.77	0.078	0.234
SUD	−0.052	0.037	−1.43	0.154	0.462
Age	0.019	0.036	0.54	0.590	1.000
Race	−0.055	0.038	−1.46	0.144	0.432
IQ	0.035	0.038	0.92	0.357	1.000
TBIs	−0.044	0.036	−1.21	0.227	0.681
Constant	−0.026	0.035	−0.74	0.462	1.000

† β-values were corrected for the three comparisons in the default network within-network optimality analysis.

Table 5
Within-Network Optimality Regression Analyses: Salience Network.

	β	Std. Err.	*t*	*p*	$p_{corrected}$ †
Efficiency Factor					
Overall model: $F(6,840) = 1.44$, $p = 0.196$					
PCL-R	−0.007	0.037	−0.20	0.840	1.000
SUD	−0.024	0.037	−0.63	0.526	1.000
Age	0.086	0.036	2.35	0.019	0.057
Race	0.009	0.038	0.23	0.819	1.000
IQ	−0.046	0.039	−1.20	0.232	0.696
TBIs	−0.027	0.037	−0.71	0.476	1.000
Constant	0.010	0.036	0.29	0.774	1.000
Vulnerability Factor					
Overall model: $F(6,840) = 0.68$, $p = 0.666$					
PCL-R	−0.002	0.034	−0.05	0.963	1.000
SUD	−0.020	0.035	−0.58	0.561	1.000
Age	−0.011	0.034	−0.33	0.743	1.000
Race	−0.038	0.036	−1.06	0.289	0.867
IQ	−0.007	0.036	−0.19	0.846	1.000
TBIs	0.059	0.035	1.71	0.087	0.261
Constant	0.025	0.034	0.75	0.451	1.000
Hubness Factor					
Overall model: $F(6,840) = 0.89$, $p = 0.499$					
PCL-R	0.031	0.038	0.81	0.420	1.000
SUD	−0.012	0.039	−0.30	0.764	1.000
Age	0.020	0.038	0.54	0.593	1.000
Race	−0.016	0.040	−0.39	0.694	1.000
IQ	−0.028	0.040	−0.71	0.479	1.000
TBIs	0.076	0.039	1.95	0.051	0.153
Constant	−0.019	0.038	−0.52	0.606	1.000

† β-values were corrected for the three comparisons in the salience network within-network optimality analysis.

Table 6
Within-Network Optimality Regression Analyses: Dorsal Attention Network.

	β	Std. Err.	*t*	*p*	$p_{corrected}$ †
Efficiency Factor					
Overall model: $F(6,840) = 2.52$, $p = 0.020$					
PCL-R	0.101*	0.037	2.75	0.006	0.018
SUD	−0.111*	0.038	−2.98	0.003	0.009
Age	0.014	0.036	0.39	0.693	1.000
Race	0.020	0.038	0.51	0.607	1.000
IQ	−0.011	0.038	−0.27	0.784	1.000
TBIs	0.009	0.037	0.25	0.802	1.000
Constant	0.014	0.036	0.39	0.696	1.000
Vulnerability Factor					
Overall model: $F(6,840) = 0.83$, $p = 0.544$					
PCL-R	−0.004	0.033	−0.12	0.905	1.000
SUD	−0.010	0.034	−0.28	0.776	1.000
Age	0.029	0.033	0.90	0.367	1.000
Race	−0.063	0.035	−1.82	0.069	0.207
IQ	−0.029	0.035	−0.83	0.408	1.000
TBIs	0.029	0.034	0.88	0.377	1.000
Constant	0.020	0.033	0.62	0.533	1.000
Hubness Factor					
Overall model: $F(6,840) = 1.96$, $p = 0.069$					
PCL-R	0.056	0.039	1.46	0.146	0.438
SUD	−0.091	0.039	−2.32	0.020	0.060
Age	0.044	0.038	1.16	0.248	0.744
Race	−0.075	0.040	−1.85	0.065	0.195
IQ	−0.028	0.040	−0.69	0.488	1.000
TBIs	−0.011	0.039	−0.27	0.788	1.000
Constant	−0.036	0.038	−0.95	0.343	1.000

† β-values were corrected for the three comparisons in the dorsal attention network within-network optimality analysis.
* $p < 0.05$ Bonferroni corrected.

Table 7
Whole-Brain Optimality Regression Analyses.

	β	Std. Err.	*t*	*p*	$p_{corrected}$ †
Efficiency Factor					
Overall model: $F(6,840) = 4.80$, $p < 0.001$					
PCL-R	0.082	0.036	2.30	0.022	0.066
SUD	−0.129*	0.036	−3.56	<0.001	0.001
Age	0.109*	0.035	3.11	0.002	0.006
Race	−0.050	0.037	−1.34	0.182	0.546
IQ	−0.015	0.037	−0.42	0.678	1.000
TBIs	−0.026	0.036	−0.72	0.472	1.000
Constant	0.014	0.035	0.40	0.689	1.000
Vulnerability Factor					
Overall model: $F(6,840) = 1.33$, $p = 0.241$					
PCL-R	0.061	0.036	1.71	0.087	0.261
SUD	0.005	0.036	0.14	0.887	1.000
Age	0.009	0.035	0.27	0.787	1.000
Race	0.007	0.037	0.20	0.841	1.000
IQ	0.075	0.037	2.02	0.044	0.132
TBIs	0.002	0.036	0.06	0.952	1.000
Constant	0.038	0.035	1.08	0.278	0.834
Hubness Factor					
Overall model: $F(6,840) = 3.60$, $p = 0.002$					
PCL-R	0.038	0.035	1.08	0.281	0.843
SUD	−0.132*	0.036	−3.65	<0.001	0.001
Age	0.063	0.035	1.80	0.072	0.216
Race	−0.061	0.037	−1.66	0.098	0.294
IQ	0.011	0.037	0.30	0.765	1.000
TBIs	−0.010	0.036	−0.29	0.772	1.000
Constant	0.002	0.035	0.07	0.945	1.000

† β-values were corrected for the three comparisons in the whole-brain optimality analysis.
* $p < 0.05$ Bonferroni corrected.

Table 8
Whole-Brain Organization Regression Analyses: Subcortical Structures.

	β	Std. Err.	*t*	*p*	$p_{corrected}$ †
Degree$_{mean_local}$					
Overall model: $F(6,840) = 1.63$, $p = 0.135$					
PCL-R	−0.067	0.036	−1.88	0.061	0.976
SUD	0.072	0.036	1.98	0.048	0.768
Age	−0.013	0.035	−0.38	0.704	1.000
Race	0.054	0.037	1.44	0.151	1.000
IQ	0.032	0.037	0.85	0.394	1.000
TBIs	−0.049	0.036	−1.36	0.175	1.000
Constant	0.019	0.035	0.55	0.584	1.000
***BC*$_{mean\_local}$**					
Overall model: $F(6,840) = 2.23$, $p = 0.038$					
PCL-R	−0.104*	0.035	−2.94	0.003	0.048
SUD	0.052	0.036	1.44	0.149	1.000
Age	−0.035	0.035	−1.00	0.317	1.000
Race	0.055	0.037	1.50	0.135	1.000
IQ	0.014	0.037	0.37	0.708	1.000
TBIs	0.031	0.036	0.86	0.390	1.000
Constant	−0.025	0.035	−0.72	0.474	1.000

† β-values were corrected for the 16 comparisons in the whole-brain optimality analysis.
* $p < 0.05$ Bonferroni corrected.

3. Results

3.1. Within-network analyses

3.1.1. Default network

PCL-R scores were not significantly related to differences in Efficiency Factor scores, β = 0.062, $p_{corrected} = 0.276$ (see Fig. 1A), Vulnerability Factor scores, β = −0.076, $p_{corrected} = 0.099$, or Hubness Factor scores, β = 0.064, $p_{corrected} = 0.234$ within the default network (see Table 4 for regressions).

3.1.2. Salience network

PCL-R scores did not significantly predict Efficiency Factor scores, β = −0.007, $p_{corrected} = 1.000$ (see Fig. 1B), Vulnerability Factor scores, β = −0.002, $p_{corrected} = 1.000$, or Hubness Factor scores, β = 0.031, $p_{corrected} = 1.000$, within the salience network (see Table 5 for regressions).

3.1.3. Dorsal attention network

Higher PCL-R scores were associated with significantly higher scores on the Efficiency Factor within the dorsal attention network, β = 0.101, $p_{corrected} = 0.018$, suggesting that inmates higher in psychopathy exhibit a more efficiently organized dorsal attention network (see Fig. 1C). Accordingly, for these inmates, neural communication within the dorsal attention network would, on average, need to travel through fewer connections (i.e., have a shorter path length) than inmates lower on psychopathy. PCL-R scores were not significantly related to either Vulnerability Factor scores, β = −0.004, $p_{corrected} = 1.000$ or Hubness Factor scores within the dorsal attention network, β = 0.056, $p_{corrected} = 0.438$ (see Table 6 for regressions).

3.2. Whole-brain analyses

3.2.1. Whole-brain optimality analysis

PCL-R scores were not significantly related to whole-brain Efficiency Factor scores, β = 0.082, $p_{corrected} = 0.066$, whole-brain Vulnerability Factor scores, β = 0.061, $p_{corrected} = 0.261$, or whole-brain Hubness Factor scores β = 0.038, $p_{corrected} = 0.843$ (see Table 7 for regressions).

3.2.2. Whole-brain organization analysis

Inmates higher on the PCL-R exhibited significant shifts in the

Table 9
Whole-Brain Organization Regression Analyses.

	Default Network				
	β	Std. Err.	*t*	*p*	$p_{corrected}$ †
Degree$_{mean_local}$					
Overall model: $F(6,840) = 0.79$, $p = 0.576$					
PCL-R	0.039	0.036	1.08	0.279	1.000
SUD	−0.013	0.036	−0.37	0.710	1.000
Age	0.048	0.035	1.36	0.176	1.000
Race	−0.001	0.037	−0.01	0.989	1.000
IQ	−0.031	0.037	−0.84	0.404	1.000
TBIs	0.038	0.036	1.04	0.296	1.000
Constant	−0.002	0.035	−0.06	0.948	1.000
***BC*$_{mean\_local}$**					
Overall model: $F(6,840) = 1.82$, $p = 0.092$					
PCL-R	−0.042	0.035	−1.20	0.231	1.000
SUD	0.054	0.036	1.51	0.132	1.000
Age	0.036	0.035	1.02	0.307	1.000
Race	0.030	0.037	0.82	0.413	1.000
IQ	−0.015	0.037	−0.41	0.682	1.000
TBIs	0.072	0.036	2.03	0.043	0.688
Constant	0.043	0.035	1.24	0.217	1.000
	Salience Network				
	β	Std. Err.	*t*	*p*	$p_{corrected}$ †
Degree$_{mean_local}$					
Overall model: $F(6,840) = 1.74$, $p = 0.108$					
PCL-R	−0.043	0.036	−1.19	0.233	1.000
SUD	−0.016	0.037	−0.43	0.669	1.000
Age	0.079	0.036	2.21	0.027	0.432
Race	0.023	0.038	0.61	0.539	1.000
IQ	0.022	0.038	0.59	0.555	1.000
TBIs	0.063	0.037	1.71	0.088	1.000
Constant	−0.006	0.036	−0.18	0.860	1.000
***BC*$_{mean\_local}$**					
Overall model: $F(6,840) = 1.20$, $p = 0.302$					
PCL-R	−0.018	0.036	−0.50	0.620	1.000
SUD	0.009	0.037	0.24	0.811	1.000
Age	0.077	0.036	2.16	0.031	0.496
Race	0.039	0.038	1.03	0.306	1.000
IQ	0.034	0.038	0.88	0.377	1.000
TBIs	0.026	0.037	0.72	0.474	1.000
Constant	0.028	0.036	0.80	0.427	1.000
	Dorsal Attention Network				
	β	Std. Err.	*t*	*P*	$p_{corrected}$ †
Degree$_{mean_local}$					
Overall model: $F(6,840) = 1.09$, $p = 0.365$					
PCL-R	−0.008	0.036	−0.23	0.820	1.000
SUD	−0.012	0.036	−0.34	0.732	1.000
Age	−0.046	0.035	−1.31	0.191	1.000
Race	−0.071	0.037	−1.92	0.055	0.880
IQ	0.008	0.037	0.21	0.837	1.000
TBIs	−0.016	0.036	−0.44	0.662	1.000
Constant	0.032	0.035	0.91	0.365	1.000
***BC*$_{mean\_local}$**					
Overall model: $F(6,840) = 2.84$, $p = 0.010$					
PCL-R	0.012	0.033	0.36	0.718	1.000
SUD	0.013	0.034	0.38	0.705	1.000
Age	−0.089	0.033	−2.73	0.006	0.096
Race	−0.074	0.034	−2.15	0.032	0.512
IQ	0.041	0.035	1.18	0.239	1.000
TBIs	−0.033	0.033	−0.98	0.329	1.000
Constant	0.094	0.032	2.91	0.004	0.064
	Cognitive Control Network				
	β	Std. Err.	*t*	*p*	$p_{corrected}$ †
Degree$_{mean_local}$					
Overall model: $F(6,840) = 1.12$, $p = 0.349$					
PCL-R	−0.019	0.036	−0.54	0.591	1.000
SUD	0.022	0.037	0.61	0.543	1.000
Age	−0.076	0.036	−2.14	0.033	0.528
Race	−0.018	0.038	−0.49	0.625	1.000
IQ	0.003	0.038	0.08	0.933	1.000
TBIs	0.042	0.036	1.15	0.250	1.000

(*continued on next page*)

Table 9 (*continued*)

	Cognitive Control Network				
	β	Std. Err.	*t*	*p*	$p_{corrected}$ †
Constant	0.028	0.035	0.80	0.423	1.000
***BC*$_{mean\_local}$**					
Overall model: $F(6,840) = 2.43$, $p = 0.025$					
PCL-R	−0.058	0.035	−1.67	0.095	1.000
SUD	0.036	0.035	1.02	0.309	1.000
Age	−0.024	0.034	−0.70	0.487	1.000
Race	0.004	0.036	0.10	0.920	1.000
IQ	0.020	0.036	0.54	0.587	1.000
TBIs	0.108*	0.035	3.09	0.002	0.032
Constant	0.080	0.034	2.36	0.018	0.288
	Somatosensory/Motor Network				
	β	Std. Err.	*t*	*p*	$p_{corrected}$ †
Degree$_{mean_local}$					
Overall model: $F(6,840) = 1.31$, $p = 0.250$					
PCL-R	0.023	0.036	0.66	0.512	1.000
SUD	0.021	0.036	0.57	0.568	1.000
Age	−0.052	0.035	−1.49	0.137	1.000
Race	0.024	0.037	0.63	0.528	1.000
IQ	−0.009	0.037	−0.23	0.820	1.000
TBIs	−0.073	0.036	−2.04	0.042	0.672
Constant	0.007	0.035	0.21	0.837	1.000
***BC*$_{mean\_local}$**					
Overall model: $F(6,840) = 3.56$, $p = 0.002$					
PCL-R	−0.029	0.036	−0.82	0.410	1.000
SUD	0.011	0.036	0.31	0.756	1.000
Age	−0.12-1*	0.035	−3.42	0.001	0.016
Race	0.050	0.037	1.34	0.182	1.000
IQ	−0.013	0.037	−0.35	0.724	1.000
TBIs	−0.083	0.036	−2.31	0.021	0.336
Constant	0.002	0.035	0.06	0.954	1.000
	Limbic Network				
	B	Std. Err.	*t*	*p*	$p_{corrected}$ †
Degree$_{mean_local}$					
Overall model: $F(6,840) = 4.49$, $p < 0.001$					
PCL-R	−0.007	0.035	−0.21	0.834	1.000
SUD	0.034	0.036	0.94	0.345	1.000
Age	0.109*	0.035	3.15	0.002	0.032
Race	−0.025	0.037	−0.68	0.498	1.000
IQ	−0.105	0.037	−2.85	0.004	0.064
TBIs	0.096	0.036	2.70	0.007	0.112
Constant	0.021	0.035	0.60	0.547	1.000
***BC*$_{mean\_local}$**					
Overall model: $F(6,840) = 4.93$, $p < 0.001$					
PCL-R	−0.029	0.035	−0.83	0.408	1.000
SUD	0.040	0.036	1.11	0.266	1.000
Age	0.103*	0.035	2.98	0.003	0.048
Race	0.017	0.037	0.46	0.647	1.000
IQ	−0.122*	0.037	−3.35	0.001	0.016
TBIs	0.078	0.035	2.20	0.028	0.448
Constant	−0.005	0.034	−0.14	0.889	1.000
	Visual Network				
	β	Std. Err.	*t*	*p*	$p_{corrected}$ †
Degree$_{mean_local}$					
Overall model: $F(6,840) = 1.85$, $p = 0.087$					
PCL-R	0.047	0.036	1.30	0.195	1.000
SUD	−0.033	0.037	−0.90	0.368	1.000
Age	−0.032	0.036	−0.88	0.379	1.000
Race	0.005	0.038	0.14	0.890	1.000
IQ	0.032	0.038	0.85	0.398	1.000
TBIs	−0.094	0.037	−2.55	0.011	0.176
Constant	0.007	0.036	0.19	0.849	1.000
***BC*$_{mean\_local}$**					
Overall model: $F(6,840) = 0.81$, $p = 0.563$					
PCL-R	0.021	0.037	0.57	0.566	1.000
SUD	0.047	0.037	1.26	0.209	1.000
Age	−0.011	0.036	−0.31	0.759	1.000
Race	0.031	0.038	0.82	0.412	1.000
IQ	0.023	0.038	0.61	0.540	1.000

Table 9 (*continued*)

	Visual Network				
	β	Std. Err.	*t*	*p*	$p_{corrected}$ †
TBIs	−0.060	0.037	−1.63	0.104	1.000
Constant	−0.005	0.036	−0.15	0.880	1.000

† β-values were corrected for the 16 comparisons in the whole-brain optimality analysis.

* $p < 0.05$ Bonferroni corrected.

overall centrality of subcortical structures in global information flow, as measured by significantly lower subcortical BC_{mean_local}, $\beta = -0.104$, $p_{corrected} = 0.048$ (see Fig. 2). More specifically, as psychopathy scores increase less information appeared to travel through subcortical structures in the global flow of information, making subcortical structures, collectively, less central to global information processing. PCL-R scores were not significantly related to $Degree_{mean\_local}$, $\beta = -0.067$, $p_{corrected} = 0.976$ (see Table 8 for regressions).

Outside of subcortical structures, PCL-R scores were not significantly related to either of the global organization metrics (i.e., $Degree_{mean\_local}$ or BC_{mean_local}) for any of the seven cortical networks examined in the whole-brain organization analysis (see Table 9 for regressions).

3.3. Supplemental analyses

Some researchers advocate for examining the subcomponent traits of psychopathy (i.e., Factor 1[interpersonal-affective] and Factor 2 [impulsive-antisocial] traits). All regression models were re-run using these subcomponent traits as simultaneous, continuous predictors. Neither Factor 1 nor Factor 2 traits significantly predicted any of the dependent variables of interest ($p_{corrected}$'s ranged from 0.147–1.000).

Similarly, psychopathy sometimes is conceptualized as a discrete clinical construct, rather than a continuous measure, with individuals scoring 30 or above on the PCL-R being characterized as psychopathic (Hare, 2003). For this analysis, inmates with PCL-R scores ≥ 30 were sorted into a "psychopathy" group ($n = 183$) and inmates with PCL-R scores ≤ 20 were sorted into a "control" group ($n = 338$; inmates exhibiting the intermediate phenotype [i.e., those with PCL-R scores between 20 and 30] were excluded from this analysis). Then, all regression models were re-run using group (contrast-coded) as a predictor. Psychopathy was associated with the same direction of effects on the efficiency factor scores within the dorsal attention network ($\beta = 0.099$, $p_{uncorrected} = .0.033$, $p_{corrected} = 0.099$) and the whole-brain subcortical BC_{mean_local} scores ($\beta = -0.120$, $p_{uncorrected} = .0.008$, $p_{corrected} = 0.128$), but neither effect was significant after correction. Group did not significantly predict any of the other dependent variables reported in the main analysis (remaining $p_{corrected}$'s ranged from 0.216–1.000). This failure to find a significant effect in this grouped analysis is likely due to the substantial drop in power from the full sample ($n = 847$) to the subsample ($n = 521$).

Following recent research examining the impact of scan length on the reliability of rs-fMRI connectivity metrics, some researchers have raised concerns about the reliability of 5-minute rs-fMRI sessions (Birn et al., 2013). We sought to address these concerns in the current study by examining the subset of the sample who completed longer rs-fMRI sessions (i.e., 10–15 min sessions; $n = 142$). Specifically, we reran all processing and analysis procedures described above (see *2. Methods and Materials*) on this subsample using the data from their entire rs-fMRI session to see whether our two significant findings replicated when data from longer rs-fMRI sessions were examined. The dorsal attention network finding replicated in the subsample; inmates higher on psychopathy were still associated with significantly higher efficiency factors scores within the dorsal attention network ($\beta = 0.198$, $p = 0.038$). Additionally, subcortical BC_{mean_local} was still

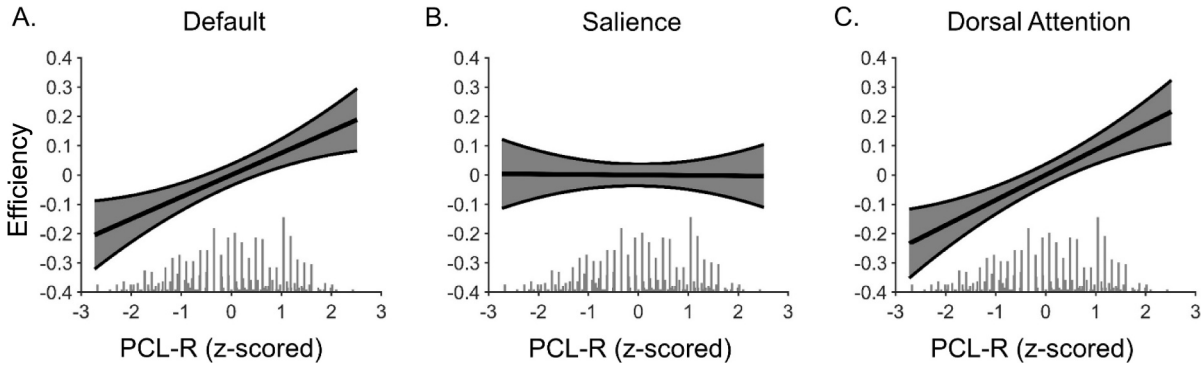

Fig. 1. Inmates higher in psychopathy showed a more efficiently organized dorsal attention network**.** Panel A displays a regression line depicting Efficiency Factor scores for the default network as a function of PCL-R total score, controlling for SUD, Race, Age, IQ, and TBI. Panel B displays a regression line depicting Efficiency Factor scores for the salience network as a function of PCL-R total score, controlling for SUD, Race, Age, IQ, and TBI. Panel C displays a regression line depicting Efficiency Factor scores for the dorsal attention network as a function of PCL-R total score, controlling for SUD, Race, Age, IQ, and TBI. Error bands represent one standard error. A dot plot of the frequency of PCL-R scores is indicated along the *x*-axis.

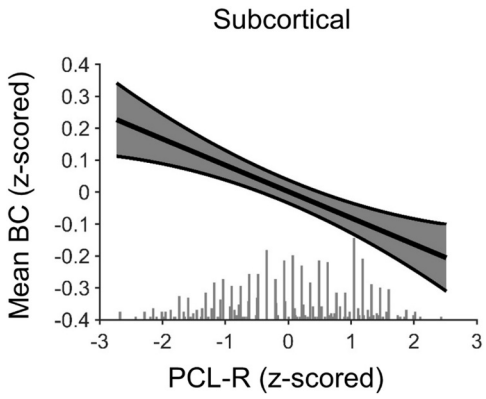

Fig. 2. Inmates higher in psychopathy showed decreased mean betweenness centrality (BC_{mean}) across subcortical structures in a whole-brain analysis. Fig. 2 displays a regression line depicting BC_{mean_local} across all subcortical structures in the whole-brain analysis as a function of PCL-R total score, controlling for SUD, Race, Age, IQ, and TBI. Error band represent one standard error. A dot plot of the frequency of PCL-R scores is indicated along the *x*-axis.

negatively associated with PCL-R scores when longer rs-fMRI sessions were examined in this subsample, however, the results were no longer significant ($\beta = -0.110$, $p = 0.212$). This difference in significance is likely due to the substantial drop in power from the full sample ($n = 847$) to the subsample ($n = 142$).

4. Discussion

The present study is the first to examine the optimality of neural network organization in psychopathy. By applying an MST analysis to rs-fMRI data, we demonstrate a link between inmates higher in psychopathy and hyper-efficient dorsal attention network organization. Additionally, we show through whole-brain analysis that subcortical structures are less centrally located within the global flow of information throughout the brain of inmates higher in psychopathy. By contrast, we did not detect any psychopathy-related effects on the organization of either the default or salience networks. These findings provide evidence that psychopathy is related to fundamental alterations in the organization of a major neural network and the brain as a whole.

The present study shows that, at rest, inmates higher in psychopathy exhibit a hyper-efficiently organized dorsal attention network. This network is implicated heavily in top-down allocation of selective attention during goal-pursuit (Corbetta and Shulman, 2002; Vossel et al., 2014). This psychopathy-related hyper-efficiency at rest suggests that, even when psychopathic individuals are not actively engaged in goal-pursuit (i.e., when they are not completing a task that may either require selective attention or otherwise evoke neural responses within this network), their dorsal attention network is intrinsically organized in a more effective manner. Based on research outside the field of psychopathy, this more efficient organization might allow for more rapid and/or less costly (i.e., more energy efficient) neural communication and information processing within that network at rest (Reijneveld et al., 2007; Smit et al., 2016; Stam and Reijneveld, 2007; Stam et al., 2014; Tewarie et al., 2015), and a more efficient engagement of attention when transitioning from rest to goal pursuit (Xiao et al., 2016; Xu et al., 2015). The connection between dorsal attention organization at rest and subsequent engagement of attention and goal-pursuit is an important avenue for future research in psychopathy. Nonetheless, the evidence of psychopathy-related dorsal attention abnormalities adds to a growing body of research that highlights attention abnormalities in psychopathy (see work by Hoppenbrouwers et al., 2015 using a visual search task, Wolf et al., 2012 using an attention blink task, and Zeier et al., 2009 using Flanker-type tasks). These abnormalities have been documented in multiple experimental settings and across multiple methodological modalities, and may be one factor contributing to the complex information processing abnormalities and behaviors characteristic of psychopathy.

While there was evidence of differences in the organization of the dorsal attention network, there was little evidence that the organization of other networks (default and salience) was disrupted in psychopathy. Psychopathy was not associated with differences in the organization of the default network. At first glance, the current null findings seem to contradict prior research linking psychopathy with abnormal neural connectivity within that network (Pujol et al., 2011; Sethi et al., 2015). However, an abnormal connection or set of connections within the default network would not necessarily alter the overall organization, or functioning, of that network as a whole (Bullmore and Sporns, 2009).

Additionally, psychopathy was not associated with shifts in the organization of the salience network. This is consistent with prior research using traditional connectivity analyses to examine neural communication within the salience network in psychopathy. Philippi et al. (2015), found that, at rest, PCL-R total scores were not significantly related to abnormal functional connectivity within the salience network. Therefore, it is possible that psychopathy may not disrupt spontaneous neural communication within the salience network. Moreover, although there is evidence of psychopathy-related impairments in automatically orienting to salient (e.g., affective) information (Hoppenbrouwers et al., 2017), it is possible that these impairments may not be driven by abnormal neural communication within the salience network, specifically. One alternative possibility is

that psychopathic individuals have an imbalance between the dorsal attention and salience networks, whereby hyper-efficient processing of goal-related information may inhibit automatic orienting to and complete integration of salient cues that are not immediately goal-relevant. Another possibility is that psychopathy-related failures in automatic orienting to salient cues may be due to breakdowns in neural communication in subcortical-cortical circuitry (e.g., amygdala-ventromedial prefrontal cortex circuitry; Blair, 2006; Kiehl, 2006). Accordingly, future research could further examine the impact of psychopathy on the optimality of neural communication, both at rest and during tasks, among cortical networks (e.g., salience and dorsal attention networks), as well as, between cortical networks and specific subcortical structures believed to play a role in automatic orienting to salient stimuli (e.g., amygdala, ventral striatum; Uddin, 2016).

At the level of overall brain organization, it appears that subcortical structures (e.g., amygdala, caudate, and hippocampus), collectively, act as less of a central hub in the global flow of information throughout the brain of individuals higher in psychopathy. More specifically, the current findings indicate that, when engaging in spontaneous, undirected cognition (i.e., at rest), less information flows through subcortical structures in psychopathic individuals. This suggests that spontaneous neural communication between cortical and subcortical structures, as a whole, may be disrupted in psychopathy. An unfortunate consequence of this organizational shift may be a limited ability of subcortical structures to influence cognition. Research connecting the centrality of subcortical structures to abnormalities in cognition (e.g., abnormalities in affective responding, reward and punishment processing, and memory; Baas et al., 2004; Eichenbaum, 2001; Knutson and Cooper, 2005) is needed in general, and specifically in the field of psychopathy. However, a shift in subcortical centrality and its potential influence on cognition is consistent with theoretical work in psychopathy (e.g., integrated emotion systems model, Blair, 2006; and paralimbic dysfunction model, Kiehl, 2006), neuroimaging work linking psychopathy to disrupted cortical-subcortical communication (e.g., blunted structural and functional connectivity between ventromedial prefrontal cortex and amygdala, Wolf et al., 2015; Yoder et al., 2015), and experimental work showing psychopathy is related to problems using affective information during moral decision-making (Koenigs et al., 2011), punishment feedback during reward-pursuit (Blair et al., 2004; Newman and Kosson, 1986), and past experiences of regret into future decisions (Baskin-Sommers et al., 2016).

The current findings provide strong evidence that psychopathy impacts the organization of neural communication within the brain. However, they must be considered in light of three limitations. First, this study was limited to examining neural network organization at rest. Accordingly, any potential links between these findings and psychopathy-related abnormalities in specific neurocognitive functions (e.g., allocation of attention, affective responding, etc.) are speculative. While there is extensive prior research demonstrating that neural communication and organization at rest is predictive of neural communication during tasks (Cole et al., 2014), neurocognitive functioning (Kong et al., 2018; Langer et al., 2012; Minati et al., 2012; Neubauer and Fink, 2009; van Den Heuvel et al., 2009; Xiao et al., 2016; Xu et al., 2015), and behavior (Kong et al., 2018; Wong et al., 2014), subsequent research is needed to explicitly link the current findings with each of these domains in psychopathy. Second, the current study used an adult male incarcerated sample, potentially limiting the generalizability of the current findings to either females or non-incarcerated community members higher in psychopathy. Finally, both neural networks and whole-brain organization are believed to arise as the result of various neurodevelopmental processes interacting throughout the course of development (Gao et al., 2015, 2009; Smit et al., 2016; Stevens et al., 2009; Uddin et al., 2010, 2011). However, the current investigation was limited to incarcerated adults. This limited our ability to evaluate at what age psychopathy-related abnormalities in neural network organization may arise, as well as what neurodevelopmental processes may be contributing to the emergence of these psychopathy-related abnormalities.

5. Conclusions

In sum, the present study provides evidence that psychopathy is related to alterations in the overall organization of neural networks. Specifically, individuals higher in psychopathy show more efficiently organized dorsal attention networks and a reduction in the centrality of subcortical structures in global information flow. These findings indicate that, even at rest, the neural architecture of psychopathy is atypical. Future research refining our understanding of this atypicality and connecting it to task and real-world behavior will serve to enhance our understanding of the neural mechanisms underlying psychopathy.

Declaration of Competing Interest

None of the authors have a conflict of interest to report.

Acknowledgements

We thank the Wisconsin and New MexicoDepartments of Corrections for their continued support. This work was supported by R01DA026964, R01MH090169, R01MH087525, 1R01DA026505, 1R01DA020870, 1R01MH070539.

Supplementary materials

Supplementary material associated with this article can be found, in the online version, at doi:10.1016/j.nicl.2019.102083.

References

Baas, D., Aleman, A., Kahn, R.S., 2004. Lateralization of amygdala activation: a systematic review of functional neuroimaging studies. Brain Res. Rev. 45, 96–103.
Baskin-Sommers, A.R., Baskin, D.R., Sommers, I.B., Newman, J.P., 2013a. The intersectionality of sex, race, and psychopathology in predicting violent crimes. Crim. Justice Behav. 40, 1068–1091.
Baskin-Sommers, A.R., Curtin, J.J., Newman, J.P., 2011a. Specifying the attentional selection that moderates the fearlessness of psychopathic offenders. Psychol. Sci. 22, 226–234.
Baskin-Sommers, A.R., Curtin, J.J., Newman, J.P., 2013b. Emotion-modulated startle in psychopathy: clarifying familiar effects. J. Abnorm. Psychol. 122, 458–468.
Baskin-Sommers, A.R., Newman, J.P., Sathasivam, N., Curtin, J.J., 2011b. Evaluating the generalizability of a fear deficit in psychopathic African American offenders. J. Abnorm. Psychol. 120, 71.
Baskin-Sommers, A.R., Stuppy-Sullivan, A.M., Buckholtz, J.W., 2016. Psychopathic individuals exhibit but do not avoid regret during counterfactual decision making. Proc. Natl. Acad.Sci. 113, 14438–14443.
Birbaumer, N., Veit, R., Lotze, M., Erb, M., Hermann, C., Grodd, W., Flor, H., 2005. Deficient fear conditioning in psychopathy: a functional magnetic resonance imaging study. Arch. Gen. Psychiatry 62, 799–805.
Birn, R.M., Molloy, E.K., Patriat, R., Parker, T., Meier, T.B., Kirk, G.R., Nair, V.A., Meyerand, M.E., Prabhakaran, V., 2013. The effect of scan length on the reliability of resting-state fMRI connectivity estimates. Neuroimage 83, 550–558.
Blair, J., 2006. The emergence of psychopathy: implications for the neuropsychological approach to developmental disorders. Cognition 101, 414–442.
Blair, J., Mitchell, D.G., Leonard, A., Budhani, S., Peschardt, K.S., Newman, C., 2004. Passive avoidance learning in individuals with psychopathy: modulation by reward but not by punishment. Pers. Individ. Dif. 37, 1179–1192.
Bullmore, E., Sporns, O., 2009. Complex brain networks: graph theoretical analysis of structural and functional systems. Nat. Rev. Neurosci. 10, 186–198.
Caeyenberghs, K., Leemans, A., Heitger, M.H., Leunissen, I., Dhollander, T., Sunaert, S., Dupont, P., Swinnen, S.P., 2012. Graph analysis of functional brain networks for cognitive control of action in traumatic brain injury. Brain 135, 1293–1307.
Calhoun, V.D., Wager, T.D., Krishnan, A., Rosch, K.S., Seymour, K.E., Nebel, M.B., Mostofsky, S.H., Nyalakanai, P., Kiehl, K.A., 2017. The impact of T1 versus EPI spatial normalization templates for fMRI data analyses. Hum. Brain Mapp. 38, 5331–5342.
Cole, M.W., Bassett, D.S., Power, J.D., Braver, T.S., Petersen, S.E., 2014. Intrinsic and task-evoked network architectures of the human brain. Neuron 83, 238–251.
Corbetta, M., Shulman, G.L., 2002. Control of goal-directed and stimulus-driven attention in the brain. Nat. Rev. Neurosci. 3, 201.
Dawel, A., O'Kearney, R., McKone, E., Palermo, R., 2012. Not just fear and sadness: meta-analytic evidence of pervasive emotion recognition deficits for facial and vocal expressions in psychopathy. Neurosci. Biobehav. Rev. 36, 2288–2304.

Decety, J., Chen, C., Harenski, C.L., Kiehl, K.A., 2013a. An fMRI study of affective perspective taking in individuals with psychopathy: imagining another in pain does not evoke empathy. Front Hum Neurosci. 7, 489.
Decety, J., Chen, C., Harenski, C.L., Kiehl, K.A., 2015. Socioemotional processing of morally-laden behavior and their consequences on others in forensic psychopaths. Hum Brain Mapp. 36, 2015–2026.
Decety, J., Skelly, L., Yoder, K.J., Kiehl, K.A., 2014. Neural processing of dynamic emotional facial expressions in psychopaths. Soc. Neurosci. 9, 36–49.
Decety, J., Skelly, L.R., Kiehl, K.A., 2013b. Brain response to empathy-eliciting scenarios involving pain in incarcerated individuals with psychopathy. JAMA Psychiatry 70, 638–645.
Deeley, Q., Daly, E., Surguladze, S., Tunstall, N., Mezey, G., Beer, D., Ambikapathy, A., Robertson, D., Giampietro, V., Brammer, M.J., 2006. Facial emotion processing in criminal psychopathy: preliminary functional magnetic resonance imaging study. Br. J. Psychiatry 189, 533–539.
Eichenbaum, H., 2001. The hippocampus and declarative memory: cognitive mechanisms and neural codes. Behav. Brain Res. 127, 199–207.
Espinoza, F.A., Vergara, V.M., Reyes, D., Anderson, N.E., Harenski, C.L., Decety, J., Rachakonda, S., Damaraju, E., Rashid, B., Miller, R.L., Koenigs, M., Kosson, D.S., Harenski, K., Kiehl, K.A., Calhoun, V.D., 2018. Aberrant functional network connectivity in psychopathy from a large (N = 985) forensic sample. Hum Brain Mapp. 39, 2624–2634.
First, M.B., Spitzer, R.L., Gibbon, M., Williams, J.B.W., 2002. Structured Clinical Interview for DSM-IV-TR axis I Disorders, Research Version, patient edition. SCID-I/P, New York, NY.
Freire, L., Mangin, J.F., 2001. Motion correction algorithms may create spurious brain activations in the absence of subject motion. Neuroimage 14, 709–722.
Freire, L., Roche, A., Mangin, J.F., 2002. What is the best similarity measure for motion correction in fMRI time series? IEEE Trans. Med. Imaging 21, 470–484.
Gao, W., Alcauter, S., Smith, J.K., Gilmore, J.H., Lin, W., 2015. Development of human brain cortical network architecture during infancy. Brain Struct. Funct. 220, 1173–1186.
Gao, W., Zhu, H., Giovanello, K., S., Smith, J.K., Shen, D., Gilmore, J.H., Lin, W., 2009. Evidence on the emergence of the brain's default network from 2-week-old to 2-year-old healthy pediatric subjects. Proc. Natl. Acad. Sci. 106, 6790–6795.
Glenn, A.L., Raine, A., Schug, R.A., 2009. The neural correlates of moral decision-making in psychopathy. Mol. Psychiatry 14, 5–6.
Gonzalez, G.F., Van der Molen, M.J., Zaric, G., Bonte, M., Tijms, J., Blomert, L., Stam, C.J., Van der Molen, M.W., 2016. Graph analysis of EEG resting state functional networks in dyslexic readers. Clin. Neurophysiol. 127, 3165–3175.
Gordon, E.M., Laumann, T.O., Adeyemo, B., Huckins, J.F., Kelley, W.M., Petersen, S.E., 2016. Generation and evaluation of a cortical area parcellation from resting-state correlations. Cereb. Cortex 26, 288–303.
Gorenstein, E.E., Newman, J.P., 1980. Disinhibitory psychopathology: a new perspective and a model for research. Psychol. Rev. 87, 301.
Hare, R.D., 2003. Manual for the Revised Psychopathy Checklist, 2 ed. Multi-Health Systems, Toronto, Ontario, Canada.
Harenski, C.L., Edwards, B.G., Harenski, K.A., Kiehl, K.A., 2014. Neural correlates of moral and non-moral emotion in female psychopathy. Front. Hum. Neurosci. 8, 741.
Hiatt, K.D., Schmitt, W.A., Newman, J.P., 2004. Stroop tasks reveal abnormal selective attention among psychopathic offenders. Neuropsychology 18, 50–59.
Hoppenbrouwers, S.S., Bulten, B.H., Brazil, I.A., 2016. Parsing fear: a reassessment of the evidence for fear deficits in psychopathy. Psychol. Bull. 142, 573.
Hoppenbrouwers, S.S., Munneke, J., Kooiman, K.A., Little, B., Neumann, C.S., Theeuwes, J., 2017. Fearful faces do not lead to faster attentional deployment in individuals with elevated psychopathic traits. J. Psychopathol. Behav. Assess. 39, 596–604.
Hoppenbrouwers, S.S., Van der Stigchel, S., Slotboom, J., Dalmaijer, E.S., Theeuwes, J., 2015. Disentangling attentional deficits in psychopathy using visual search: failures in the use of contextual information. Pers. Individ. Dif. 86, 132–138.
Hyde, L.W., Byrd, A.L., Votruba-Drzal, E., Hariri, A.R., Manuck, S.B., 2014. Amygdala reactivity and negative emotionality: divergent correlates of antisocial personality and psychopathy traits in a community sample. J. Abnorm. Psychol. 123, 214–224.
Itahashi, T., Yamada, T., Watanabe, H., Nakamura, M., Jimbo, D., Shioda, S., Toriizuka, K., Kato, N., Hashimoto, R., 2014. Altered network topologies and hub organization in adults with autism: a resting-state fMRI study. PLoS ONE 9, e94115.
Jack, A.I., Dawson, A.J., Begany, K.L., Leckie, R.L., Barry, K.P., Ciccia, A.H., Snyder, A.Z., 2013. fMRI reveals reciprocal inhibition between social and physical cognitive domains. Neuroimage 66, 385–401.
Kiehl, K.A., 2006. A cognitive neuroscience perspective on psychopathy: evidence for paralimbic system dysfunction. Psychiatry Res. 142, 107–128.
Kiehl, K.A., Hoffman, M.B., 2011. The criminal psychopath: history, neuroscience, treatment, and economics. Jurimetrics 51, 355.
King, N.S., Crawford, S., Wenden, F.J., Moss, N.E.G., Wade, D.T., 1995. The rivermead post concussion symptoms questionnaire: a measure of symptoms commonly experienced after head injury and its reliability. J. Neurol. 242, 587–592.
Knutson, B., Cooper, J.C., 2005. Functional magnetic resonance imaging of reward prediction. Curr. Opin. Neurol. 18, 411–417.
Koenigs, M., Kruepke, M., Zeier, J.D., Newman, J.P., 2011. Utilitarian moral judgment in psychopathy. Soc. Cogn. Affect. Neurosci. 7, 708–714.
Kong, R., Li, J., Orban, C., Sabuncu, M.R., Liu, H., Schaefer, A., Sun, N., Zuo, X.N., Holmes, A.J., Eickhoff, S.B., Yeo, B.T.T., 2018. Spatial topography of individual-specific cortical networks predicts human cognition, personality, and emotion. Cereb. Cortex 29, 2533–2551.
Kruskal, J.B., 1956. On the shortest spanning subtree of a graph and the traveling salesman problem. Proc. Am. Math. Soc. 7, 48–50.
Langer, N., Pedroni, A., Gianotti, L.R.R., Hänggi, J., Knoch, D., Jäncke, L., 2012. Functional brain network efficiency predicts intelligence. Hum. Brain Mapp. 33, 1393–1406.
Larson, C.L., Baskin-Sommers, A.R., Stout, D.M., Balderston, N.L., Curtin, J.J., Schultz, D.H., Kiehl, K.A., Newman, J.P., 2013. The interplay of attention and emotion: top-down attention modulates amygdala activation in psychopathy. Cogn. Affect. Behav. Neurosci. 13, 757–770.
Lindner, P., Flodin, P., Budhiraja, M., Savic, I., Jokinen, J., Tiihonen, J., Hodgins, S., 2018. Associations of psychopathic traits with local and global brain network topology in young adult women. Biol. Psychiatry: Cogn. Neurosci. Neuroimaging 3, 1003–1012.
Liu, J., Liang, J., Qin, W., Tian, J., Yuan, K., Bai, L., Zhang, Y., Wang, W., Wang, Y., Li, Q., Zhao, L., Lu, L., von Deneen, K.M., Liu, Y., Gold, M.S., 2009. Dysfunctional connectivity patterns in chronic heroin users: an fMRI study. Neurosci. Lett. 460, 72–77.
Liu, Y., Liang, M., Zhou, Y., He, Y., Hao, Y., Song, M., Yu, C., Liu, H., Liu, Z., Jiang, T., 2008. Disrupted small-world networks in schizophrenia. Brain 131, 945–961.
Lykken, D.T., 1957. A study of anxiety in the sociopathic personality. J. Abnorm. Psychol. 55, 6–10.
Mazaika, P.K., Hoeft, F., Glover, G.H., Reiss, A.L., 2009. Methods and software for fMRI analysis of clinical subjects. Neuroimage 47, S58.
Meffert, H., Gazzola, V., den Boer, J.A., Bartels, A.A., Keysers, C., 2013. Reduced spontaneous but relatively normal deliberate vicarious representations in psychopathy. Brain 136, 2550–2562.
Minati, L., Grisoli, M., Seth, A.K., Critchley, H.D., 2012. Decision-making under risk: a graph-based network analysis using functional MRI. Neuroimage 60, 2191–2205.
Neubauer, A.C., Fink, A., 2009. Intelligence and neural efficiency. Neurosci. Biobehav. Rev. 33, 1004–1023.
Neumann, C.S., Hare, R.D., 2008. Psychopathic traits in a large community sample: links to violence, alcohol use, and intelligence. J. Consult. Clin. Psychol. 76, 893–899.
Newman, J.P., Curtin, J.J., Bertsch, J.D., Baskin-Sommers, A.R., 2010. Attention moderates the fearlessness of psychopathic offenders. Biol. Psychiatry 67, 66–70.
Newman, J.P., Kosson, D.S., 1986. Passive avoidance learning in psychopathic and nonpsychopathic offenders. J. Abnorm. Psychol. 95, 252.
Pandit, A.S., Expert, P., Lambiotte, R., Bonnelle, V., Leech, R., Turkheimer, F.E., Sharp, D.J., 2013. Traumatic brain injury impairs small-world topology. Neurology 80, 1826–1833.
Patrick, C.J., Bradley, M., Lang, P., 1993. Emotion in the criminal psychopath: startle reflex modulation. J. Abnorm. Psychol. 102, 82–92.
Pauli, W.M., Nili, A., .N, Tyszka, J.M., 2018. A high-resolution probabilistic in vivo atlas of human subcortical brain nuclei. Sci Data 5, 180063.
Philippi, C.L., Pujara, M.S., Motzkin, J.C., Newman, J.P., Kiehl, K.A., Koenigs, M., 2015. Altered resting-state functional connectivity in cortical networks in psychopathy. J.Neurosci. 35, 6068–6078.
Power, J.D., Mitra, A., Laumann, T.O., Snyder, A.Z., Schlaggar, B.L., Petersen, S.E., 2014. Methods to detect, characterize, and remove motion artifact in resting state fMRI. Neuroimage 84, 320–341.
Pujol, J., Batalla, I., Contreras-Rodríguez, O., Harrison, B.J., Pera, V., Hernández-Ribas, R., Real, E., Bosa, L., Soriano-Mas, C., Deus, J., 2011. Breakdown in the brain network subserving moral judgment in criminal psychopathy. Soc. Cogn. Affect Neurosci. 7, 917–923.
Reijneveld, J.C., Ponten, S.C., Berendse, H.W., Stam, C.J., 2007. The application of graph theoretical analysis to complex networks in the brain. Clin. Neurophysiol. 118, 2317–2331.
Sadeh, N., Verona, E., 2012. Visual complexity attenuates emotional processing in psychopathy: implications for fear-potentiated startle deficits. Cogn. Affect. Behav. Neurosci. 12, 346–360.
Schaefer, A., Kong, R., Gordon, E.M., Laumann, T.O., Zuo, X.N., Holmes, A.J., Eickhoff, S.B., Yeo, B.T.T., 2018. Local-global parcellation of the human cerebral cortex from intrinsic functional connectivity MRI. Cereb. Cortex 28, 3095–3114.
Schultz, D.H., Balderston, N.L., Baskin-Sommers, A.R., Larson, C.L., Helmstetter, F.J., 2016. Psychopaths show enhanced amygdala activation during fear conditioning. Front. Psychol. 7, 348.
Sethi, A., Gregory, S., Dell'Acqua, F., Thomas, E.P., Simmons, A., Murphy, D.G.M., Hodgins, S., Blackwood, N.J., Craig, M.C., 2015. Emotional detachment in psychopathy: involvement of dorsal default-mode connections. Cortex 62, 11–19.
Siegel, J.S., Mitra, A., Laumann, T.O., Seitzman, B.A., Raichle, M., Corbetta, M., Snyder, A.Z., 2016. Data quality influences observed links between functional connectivity and behavior. Cereb. Cortex 27, 4492–4502.
Sjoerds, Z., Stufflebeam, S.M., Veltman, D.J., Van den Brink, W., Penninx, B.W.J.H., Douw, L., 2017. Loss of brain graph network efficiency in alcohol dependence. Addict. Biol. 22, 523–534.
Smit, D.J., de Geus, E.J., Boersma, M., Boomsma, D.I., Stam, C.J., 2016. Life-span development of brain network integration assessed with phase lag index connectivity and minimum spanning tree graphs. Brain Connect. 6, 312–325.
Sommer, M., Sodian, B., Dohnel, K., Schwerdtner, J., Meinhardt, J., Hajak, G., 2010. In psychopathic patients emotion attribution modulates activity in outcome-related brain areas. Psychiatry Res. 182, 88–95.
Spreng, R.N., Grady, C.L., 2010. Patterns of brain activity supporting autobiographical memory, prospection, and theory of mind, and their relationship to the default mode network. J. Cogn. Neurosci. 22, 1112–1123.
Spreng, R.N., Mar, R.A., Kim, A., 2009. The common neural basis of autobiographical memory, prospection, navigation, theory of mind, and the default mode: a quantitative meta-analysis. J. Cogn. Neurosci. 21, 489–510.
Stam, C.J., Reijneveld, J.C., 2007. Graph theoretical analysis of complex networks in the brain. Nonlinear Biomed. Phys. 1, 3.
Stam, C.J., Tewarie, P., Van Dellen, E., van Straaten, E.C., Hillebrand, A., Van Mieghem, P., 2014. The trees and the forest: characterization of complex brain networks with

minimum spanning trees. Int. J. Psychophysiol. 92, 129–138.
Stevens, M.C., Pearlson, G.D., Calhoun, V.D., 2009. Changes in the interaction of resting-state neural networks from adolescence to adulthood. Hum. Brain Mapp. 30, 2356–2366.
Tewarie, P., van Dellen, E., Hillebrand, A., Stam, C.J., 2015. The minimum spanning tree: an unbiased method for brain network analysis. Neuroimage 104, 177–188.
Tillem, S., Baskin-Sommers, A.R., 2018. Individuals with psychopathic traits view distracting neutral information as negatively valenced. Int. J. Forensic Ment. Health 17, 25–34.
Tillem, S., Brennan, G.M., Wu, J., Mayes, L.C., Baskin-Sommers, A.R., 2019. Alpha response reveals attention abnormalities in psychopathy. Personal. Disord. Theory, Res. Treat. 10, 291–296.
Tillem, S., Ryan, J., Wu, J., Crowley, M.J., Mayes, L.C., Baskin-Sommers, A.R., 2016. Theta phase coherence in affective picture processing reveals dysfunctional sensory integration in psychopathic offenders. Biol. Psychol. 119, 42–45.
Tillem, S., van Dongen, J., Brazil, I.A., Baskin-Sommers, A., 2018. Psychopathic traits are differentially associated with efficiency of neural communication. Psychophysiology 55, e13194.
Tzourio-Mazoyer, N., Landeau, B., Papathanassiou, D., Crivello, F., Etard, O., Delcroix, N., Mazoyer, B., Joliot, M., 2002. Automated anatomical labeling of activations in SPM using a macroscopic anatomical parcellation of the MNI MRI single-subject brain. Neuroimage 15, 273–289.
Uddin, L.Q., 2016. Salience Network of the Human Brain. Academic press.
Uddin, L.Q., Supekar, K.S., Menon, V., 2010. Typical and atypical development of functional human brain networks: insights from resting-state FMRI. Front. Syst. Neurosci. 4, 21.
Uddin, L.Q., Supekar, K.S., Ryali, S., Menon, V., 2011. Dynamic reconfiguration of structural and functional connectivity across core neurocognitive brain networks with development. J. Neurosci. 31, 18578–18589.
Vaidyanathan, U., Hall, J.R., Patrick, C.J., Bernat, E.M., 2011. Clarifying the role of defensive reactivity deficits in psychopathy and antisocial personality using startle reflex methodology. J. Abnorm. Psychol. 120, 253.
van Den Heuvel, M.P., Stam, C.J., Kahn, R.S., Hulshoff Pol, H.E., 2009. Efficiency of functional brain networks and intellectual performance. J. Neurosci. 29, 7619–7624.
Vossel, S., Geng, J.J., Fink, G.R., 2014. Dorsal and ventral attention systems: distinct neural circuits but collaborative roles. The Neurosci. 20, 150–159.
Wechsler, D., 1997. WAIS-3: Wechsler Adult Intelligence Scale: Administration and scoring manual. The Psychological Corporation. San Antonio, TX, USA.
Whitfield-Gabrieli, S., Nieto-Castanon, A., 2012. Conn: a functional connectivity toolbox for correlated and anticorrelated brain networks. Brain Connect. 2, 125–141.
Wilkinson, G.S., 1993. WRAT-3: Wide Range Achievement Test Administration Manual. Wide Range incorporated.
Wilson, K., Juodis, M., Porter, S., 2011. Fear and loathing in psychopaths: a meta-analytic investigation of the facial affect recognition deficit. Crim. Justice Behav. 38, 659–668.
Wolf, R.C., Carpenter, R.W., Warren, C.M., Zeier, J.D., Baskin-Sommers, A.R., Newman, J.P., 2012. Reduced susceptibility to the attentional blink in psychopathic offenders: implications for the attention bottleneck hypothesis. Neuropsychology 26, 102–109.
Wolf, R.C., Pujara, M.S., Motzkin, J.C., Newman, J.P., Kiehl, K.A., Decety, J., Kosson, D.S., Koenigs, M., 2015. Interpersonal traits of psychopathy linked to reduced integrity of the uncinate fasciculus. Hum. Brain Mapp. 36, 4202–4209.
Wong, C.W., Olafsson, V., Plank, M., Snider, J., Halgren, E., Poizner, H., Liu, T.T., 2014. Resting-state fMRI activity predicts unsupervised learning and memory in an immersive virtual reality environment. PLoS ONE 9, e109622.
Xiao, M., Ge, H., Khundrakpam, B.S., Xu, J., Bezgin, G., Leng, Y., Zhao, L., Tang, Y., Ge, X., Jeon, S., 2016. Attention performance measured by attention network test is correlated with global and regional efficiency of structural brain networks. Front. Behav. Neurosci. 10, 194.
Xu, J., Yin, X., Ge, H., Han, Y., Pang, Z., Tang, Y., Liu, B., Liu, S., 2015. Attentional performance is correlated with the local regional efficiency of intrinsic brain networks. Front. Behav. Neurosci. 9, 200.
Yang, Y., Raine, A., Joshi, A.A., Joshi, S., Chang, Y.T., Schug, R.A., Wheland, D., Leahy, R., Narr, K.L., 2012. Frontal information flow and connectivity in psychopathy. The Br. J. Psychiatry 201, 408–409.
Yeo, B.T., Krienen, F.M., Sepulcre, J., Sabuncu, M.R., Lashkari, D., Hollinshead, M., Roffman, J.L., Smoller, J.W., Zollei, L., Polimeni, J.R., Fischl, B., Liu, H., Buckner, R.L., 2011. The organization of the human cerebral cortex estimated by intrinsic functional connectivity. J. Neurophysiol. 106, 1125–1165.
Yoder, K.J., Harenski, C.L., Kiehl, K.A., Decety, J., 2015. Neural networks underlying implicit and explicit moral evaluations in psychopathy. Transl. Psychiatry 5, e625.
Zeier, J.D., Maxwell, J.S., Newman, J.P., 2009. Attention moderates the processing of inhibitory information in primary psychopathy. J. Abnorm. Psychol. 118, 554–563.